Data in Brief 38 (2021) 107369

Contents lists available at ScienceDirect

Data in Brief

journal homepage: www.elsevier.com/locate/dib

Data Article

Structural, energetic and kinetic database of catalytic reactions: Benzyl alcohol to benzaldehyde oxidation on MnO_x clusters

Laura Gueci[a], Francesco Ferrante[a], Antonio Prestianni[a], Francesco Arena[b], Dario Duca[a,*]

[a] Università degli Studi di Palermo, Dipartimento di Fisica e Chimica "Emilio Segrè", viale delle scienze ed. 17, Palermo 90128, Italy
[b] Università degli Studi di Messina, Dipartimento di Ingegneria, Contrada Di Dio, S. Agata 98166, Messina, Italy

ARTICLE INFO

Article history:
Received 21 July 2021
Revised 2 September 2021
Accepted 9 September 2021
Available online 13 September 2021

Keywords:
MnO_x
Oxidative–dehydrogenation
Deactivation
Remediation
DFT
Reaction kinetic

ABSTRACT

Data here reported are connected with the research article "Benzyl Alcohol to Benzaldehyde Oxidation on MnO_x Clusters: Unraveling Atomistic Features" Gueci et al. [1]. This work described and discussed structural and energetic results, calculated by Density Functional Theory (DFT). In order to get kinetic information, DFT results were refined by an original approach, which will be shortly described in the following article. The crossed analysis of experimental and computational energetic and kinetic data allowed to (i) reconstruct the complicated lattice that connects the primary and secondary mechanisms of the reaction and (ii) identify alternative process pathways capable of by-passing parasitic mechanisms, decreasing selectivity. On the other hand, the data here presented show what is the basic information necessary to obtain the modeling of a complex process of heterogeneous catalysis. Moreover, they can be used either to verify the validity of the discussion outlined in the original article Gueci et al. [1] or as a starting point to computationally explore alternative routes and the related kinetics of the same oxidation processes, in the aim to further optimize the corresponding experimental approach.

DOI of original article: 10.1016/j.mcat.2021.111735
* Corresponding author.
E-mail address: dario.duca@unipa.it (D. Duca).

https://doi.org/10.1016/j.dib.2021.107369

Specifications Table

Subject	Chemistry
Specific subject area	Catalytic Computational Chemistry
Type of data	Table Graph Figure
How data were acquired	Calculations: • electronic structure in DFT frames (M06-L exchange correlation functional, Stuttgart '97 Relativistic Small Core effective potential and cc-pVDZ basis sets), starting by tentative Cartesian coordinates; • linear algebra applications, using the energetic information obtained by the calculations above to outline kinetic data. Hardware: • dedicated Linux computer cluster, assembled by x86 (Xeon and Opteron) and IA64 processors, characterized by about 3 TB RAM, more than 24 TB Total-Storage and with a Computation Power larger than 13 Tflop/s. Software: • Gaussian 09 suite of programs, Revision D.01 by Gaussian Inc. Wallingford CT 2009, for the electronic structure calculations; • Computer Algebra System Maxima, version 5.45.0, for the application of the Simplified Christiansen Method (SCM).
Data format	Raw Analyzed
Parameters for data collection	The Molden open source graphical molecular editor, version 5.8, was used to build the input geometries for the electronic structure calculations and to analyze the output geometries and vibrational normal modes.
Description of data collection	DFT optimized geometries and vibrational zero-point corrected electronic energies were obtained by Gaussian 09 suite of programs, employing the High Performance Computing dedicated resources of the Palermo Computational Chemistry Center (CCCP) group, allocated at the Dipartimento di Fisica e Chimica "Emilio Segrè" dell'Università di Palermo (DiFC-UNIPA).
Data source location	Institution: DiFC-UNIPA City/Region: Palermo/Sicily Country: Italy
Data accessibility	Data are included with the article and, as supplementary material (optimized Cartesian xyz-coordinate structures and the related absolute ZPVE/E_h values), in a separated file.
Related research article	L. Gueci, F. Ferrante, A. Prestianni, F. Arena, D. Duca, Benzyl alcohol to benzaldehyde oxidation on MnO_x clusters: unraveling atomistic features, *Molecular Catalysis* 513 (2021) 111735. https://doi.org/10.1016/j.mcat.2021.111735

Value of the Data

- DFT optimized structural (xyz-coordinates) and energetic data of species (reagents, intermediates, transition states and products) involved in the catalytic oxidative dehydrogenation of benzyl alcohol to benzaldehyde on MnO_x clusters are provided along with the calculated surface populations, occurrence probabilities and other kinetic descriptors of the corresponding elementary reaction steps and whole reaction mechanisms at given temperatures.

- Data are useful for modeling material chemistry and general chemistry researchers; specifically, for those involved in computational as well as in experimental catalysis.
- Data can be used for verification of published results [1]. They can also be used both by experimental researchers in the catalytic field (to implement modeling predictions thus to optimize the reductive oxidation process by increasing the selectivity of the process) and by modeling and computational researchers (as a starting point for further mapping either the title process, which is of recognized industrial interest, or other surface processes).
- The selective oxidation of alcohols, of which benzyl alcohol to benzaldehyde oxidation on MnO_x is an example, to the corresponding carbonyl compounds is an important class of industrial reactions for the production of fine chemicals. The optimization of the catalytic reaction, related to the reported data and operatively obtained by reducing production times and increasing process selectivity, reduces its costs and environmental impact.
- Permanganate and dichromate, are usually employed for manufacturing benzaldehyde. This process however is affected by high costs and co-generation of toxic wastes. The Green Chemistry guidelines for the oxidation of benzyl alcohol, using supported noble-metal catalysts are also biased by high costs and catalytic deactivation phenomena, which could be overcome by using MnO_x based catalysts whose kinetic data are here reported.
- The suggested wholly in silico experimental design, exemplified for a potentially polluting process, adds value to the research which is actually carried out, in a first preliminary phase, without risk for the researcher and without the use of reagents and the production of derivatives of potential hazard.

1. Data Description

1.1. Structural and energetic data

The intermediate species and transition states characterizing the title reaction surface mechanisms, later in the text indicated as **M4** and **M5**: $\Phi CH_2OH \rightarrow [Mn_4O_9]\Phi CHO$, are shown in Figs. 1 and 2. The spin multiplicity and the zero point corrected energy (ZPVE) values of the optimized structures are also outlined. Details on the calculations are described in Section 2.1. Optimized xyz-coordinates are reported as electronic supplementary information (ESI), see

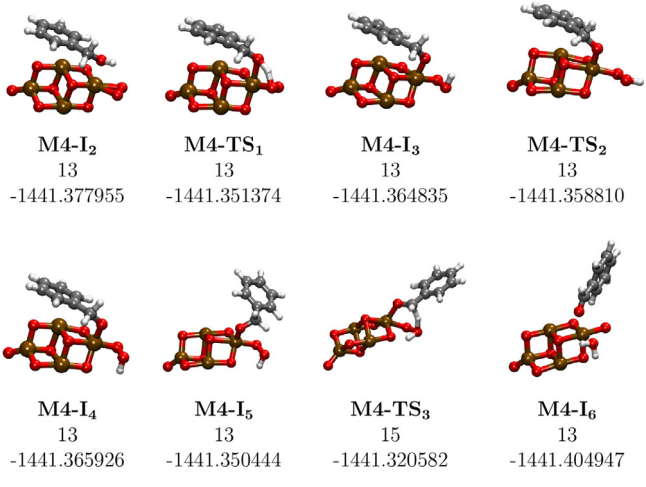

Fig. 1. Optimized fragment structure of the intermediate surface species I_m and transition states TS_n involved in the reaction mechanism **M4**: spin multiplicity $(2S+1)$ characterizing the fragments and the ZPVE/hartree values are given in the order under any structure. The reagent before adsorption and product after desorption are not shown (see text).

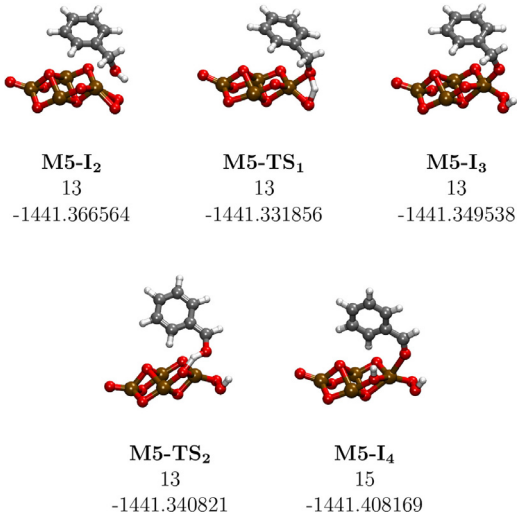

Fig. 2. Optimized fragment structure of the intermediate surface species I_m and transition states TS_n involved in the reaction mechanism **M5**: spin multiplicity $(2S+1)$ characterizing the fragments and the ZPVE/hartree values are given in the order under any structure. The reagent and product before adsorption and after desorption, respectively, are not shown.

Section 1.3. Taking the I_2 species as the reference of a given mechanism **M** and considering a generic intermediate I_i, belonging to the same mechanism, the relative energy values reported in Table 1 (under the column $\mathbf{I_i}$) could be obtained by the ZPVE values using Eq. (1):

$$\Delta E(\mathrm{I_i})\ [\mathrm{kJ\ mol^{-1}}] = 2625.5 \cdot [\mathrm{ZPVE}(I_i) - \mathrm{ZPVE}(I_2)]\ [hartree] \tag{1}$$

Conversely, the energy barrier of the sth elementary step of a given mechanism (singly reported in columns **TS** of Table 1) is calculated by Eq. (2):

$$E_b(s)\ [\mathrm{kJ\ mol^{-1}}] = 2625.5 \cdot [\mathrm{ZPVE}(TS_s) - \mathrm{ZPVE}(I_s)]\ [hartree] \tag{2}$$

being I_s the reactant of the considered step in the forward direction.

Spin multiplicity and energetic details on the optimized intermediate species and transition states characterizing the title reaction surface mechanisms **M6, M7** and **M8**: $(\Phi\mathrm{CHO} + H_2O)/Mn_4O_8 \rightarrow 2H/Mn_4O_8 + \Phi\mathrm{COOH}$, are given in Fig. 3. For the corresponding optimized xyz-coordinates, see Section 1.3 while for the differential energetics and the kinetic data Table 1.

Spin multiplicity and energetic details on the optimized intermediates and transition state characterizing the CO oxidation on one MnO_x fragment **M9**: $CO + Mn_4O_9 \rightarrow CO_2 + Mn_4O_8$, are given in Fig. 4. For the corresponding optimized xyz-coordinates, see Section 1.3 while for the differential energetics and the kinetic data Table 1.

Potentially parasitic pathway branches, in any case, hardly to occur due to either the energetic or steric properties involved, have been individuated for the title reaction. These are discussed in the connected article [1] and illustrated below by Figs. 5–7. The xyz-coordinates of the optimized structures are collected as ESI, see Section 1.3.

1.2. Kinetic data

Table 1 shows the energetics involved in the different mechanisms along with the corresponding reaction rates, s, and intermediate species, showing the largest surface molar fraction,

Table 1
Energetics (E) of reagents (R) and products (P) on free active surface sites (Ω) and of transition states (TS) and surface intermediates (I_i), characterizing the kinetic mechanisms of the title reaction along with the species showing the largest surface molar ratio (Θ) into a given mechanism (M) and the corresponding reaction rate (s) at 398 K.

	E/kJ mol^{-1}																		
M[a]	R + Ω	I_2	TS[b]	I_3	TS	I_4	TS	I_5	TS	I_6	TS	I_7	TS	I_8	TS	I_9	P + Ω	Θ[c]	s[d]/s^{-1}
M1	+153.0	0	38.1	+6.2	73.5	−84.6	–	–	–	–	–	–	–	–	–	–	+26.2	I_4	2.3×10^{-2}
M2	+87.6	0	33.1	+14.2	60.8	−23.8	–	–	–	–	–	–	–	–	–	–	+94.9	I_4	2.2×10^{-3}
M3	+190.0	0	53.3	+41.6	7.3	−249.8	–	–	–	–	–	–	–	–	–	–	−18.1	I_4	3.1×10^{-18}
M4	+165.4	0	69.8	+34.4	15.8	+31.6	–	+72.2	78.2	−154.2	–	–	–	–	–	–	−74.5	I_2	1.5×10^{-7}
M5	+135.5	0	91.1	+44.7	22.9	−109.2	–	–	–	–	–	–	–	–	–	–	−51.6	I_2	9.0×10^{0}
M6	+231.7	0	63.4	+13.8	74.5	+55.4	–	+81.5	45.3	−109.8	–	–	–	–	–	–	+82.3	I_6	4.9×10^{-13}
M7	+231.7	0	63.4	+13.8	74.5	+55.4	–	+83.9	48.8	−132.6	–	–	–	–	–	–	+49.2	I_6	1.1×10^{-11}
M8	+231.7	0	63.4	+13.8	74.5	+55.4	–	+59.1	40.4	+58.1	–	+54.9	111.7	+85.5	–	−51.0	+130.1	I_9	1.1×10^{-11}
M9	+135.5	0	104.2	−277.1	–	–	–	–	–	–	–	–	–	–	–	–	−220.0	I_2	1.7×10^{-1}

[a] **M** represents a generic mechanism. Note that the following naming of the **M** terms is the same and represent the same mechanisms in the connected article [1]:
M1 see below – $\Phi CH_2OH \rightarrow [Mn_4O_8]\Phi CHO$
M2 see below – $H_2/Mn_4O_8 + O_2 \rightarrow H_2O + Mn_4O_9$
M3 see below – $\Phi CH_2OH \rightarrow [Mn_4O_9]\Phi CHO$
M4 Fig. 1 – $\Phi CH_2OH \rightarrow [Mn_4O_9]\Phi CHO$
M5 Fig. 2 – $\Phi CH_2OH \rightarrow [Mn_4O_9]\Phi CHO$
M6 Fig. 3 – $(\Phi CHO + H_2O)/Mn_4O_8 \rightarrow 2H/Mn_4O_8 + \Phi COOH$
M7 Fig. 3 – $(\Phi CHO + H_2O)/Mn_4O_8 \rightarrow 2H/Mn_4O_8 + \Phi COOH$
M8 Fig. 3 – $(\Phi CHO + H_2O)/Mn_4O_8 \rightarrow 2H/Mn_4O_8 + \Phi COOH$
M9 Fig. 4 – $CO + Mn_4O_9 \rightarrow CO_2 + Mn_4O_8$
M1, M2, M3 mechanisms are, in the order, represented in (and discussed by) Figs. 3, 5 and 6 in reference [2].
[b] TSs are not indexed conversely to what done in the figures. The indices have to be considered sequential and ordered, i.e. to the first TS corresponds TS_1 to the second TS_2 etc.
[c] The intermediate species showing the largest accumulation (molar ratio) on the surface.
[d] Reaction rate is expressed in molecule converted per unit of time per catalytic fragment.

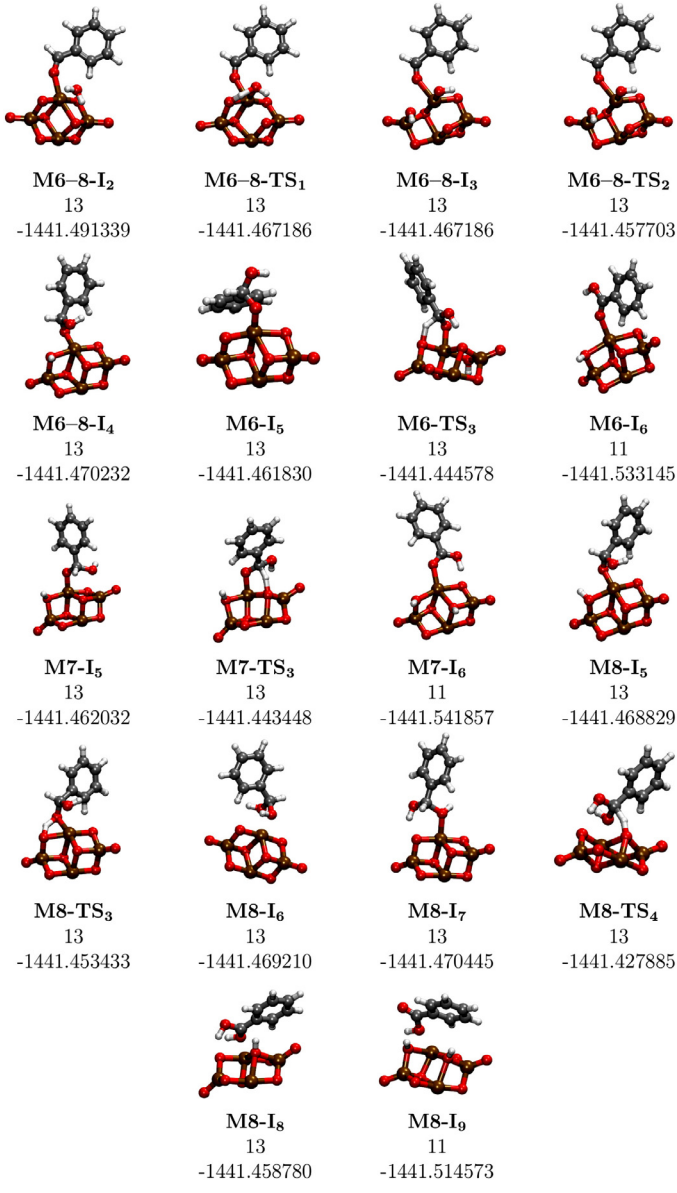

Fig. 3. Optimized fragment structure of the intermediate surface species I_m and transition states TS_n involved in the reaction mechanism **M6, M7** and **M8**: spin multiplicity $(2S+1)$ characterizing the fragments and the ZPVE/hartree values are given in the order under any structure. **M6–M8** labels indicate surface species and transition states common to the three mechanisms. Reagents and products before adsorption and after desorption, respectively, are not shown.

Θ. Both the latter were obtained by *SCM* (see Section 2.2) at 398 K and are here shown as different examples with respect to the results reported by Gueci et al. [1,2]. The zero point corrected energy data employed to obtain the relative energy values reported in Table 1 are set out in Section 1.1, Figs. 1–4, or refer to already published information [1,2].

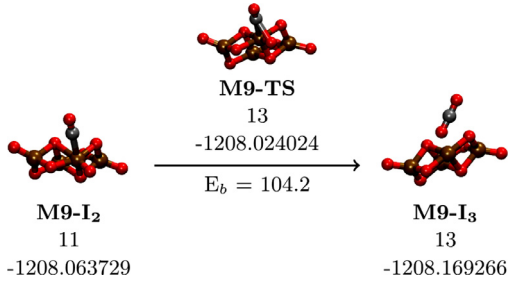

Fig. 4. Energetic profile graph with the optimized fragments of the intermediate surface species I_m and transition state TS_n involved in the CO oxidation mechanism **M9**: spin multiplicity $(2S+1)$ characterizing the fragments and the ZPVE/hartree values are given in the order under any structure. E_b is the energy barrier, i.e. the energy gap to get TS, see Eq. (1) and Table 1. The reagent before adsorption and product after desorption, are not shown.

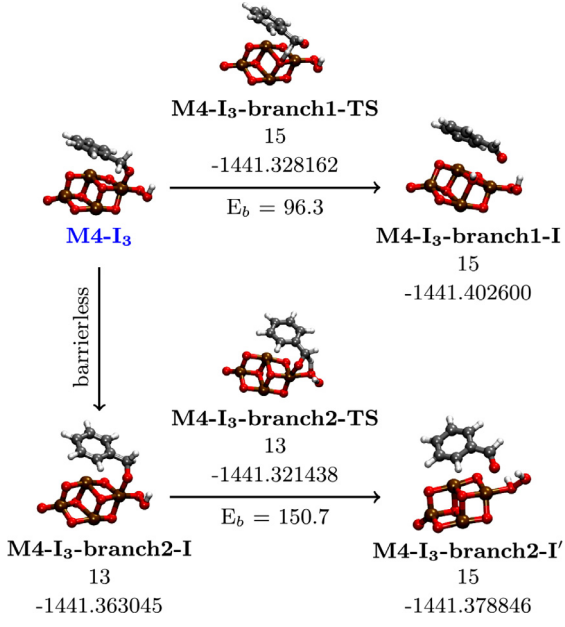

Fig. 5. Energetic profile graph with the optimized fragments of the intermediate surface species I_m and transition states TS_n involved in parasitic mechanisms: spin multiplicity $(2S+1)$ characterizing the fragments and the ZPVE/hartree values are given in the order under any structure. E_b is the energy barrier, i.e. the energy gap to get TS, see Eq. (1). Pathway mechanism and intermediate from which starts the parasitic route are highlighted in blue. (For interpretation of the references to color in this figure legend, the reader is referred to the web version of this article.)

The energy of the first adsorbed species (reference species) is arbitrarily taken equal to 0 kJ mol^{-1}. The energy for any TS is reported with respect to the energy value of the just preceding species. For the minima, the relative energy is set with respect to the species taken as a reference in the pathway involved. For the sake of consistency this procedure also applies to the $P+\Omega$ ending constellation. Therefore, the desorption energies, which usually do not appear in the pathway energy profiles [1,2] and, namely, in Figs. 1–4, correspond to the energy difference between that of the last intermediate species and that of the $P+\Omega$ system.

The energetic values shown in Table 1, as highlighted in its notes, can be obtained (mechanisms **M4**–**M9**) from Figs. 1–4 of Section 1.1, following Eq. (1), or are referred (mechanisms **M1**–**M3**) to processes already published [2] and reconsidered in the here connected article [1].

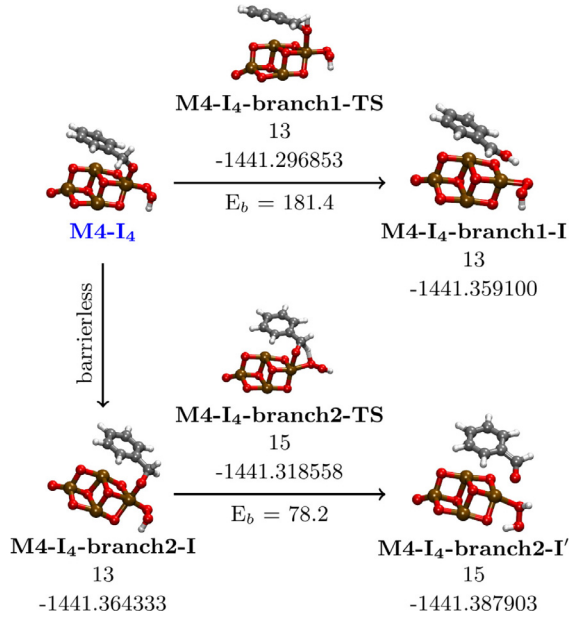

Fig. 6. Energetic profile graph with the optimized fragments of the intermediate surface species I_m and transition states TS_n involved in parasitic mechanisms: spin multiplicity $(2S+1)$ characterizing the fragments and the ZPVE/hartree values are given in the order under any structure. E_b is the energy barrier, i.e. the energy gap to get TS, see Eq. (1). Pathway mechanism and intermediate from which starts the parasitic route are highlighted in blue. (For interpretation of the references to color in this figure legend, the reader is referred to the web version of this article.)

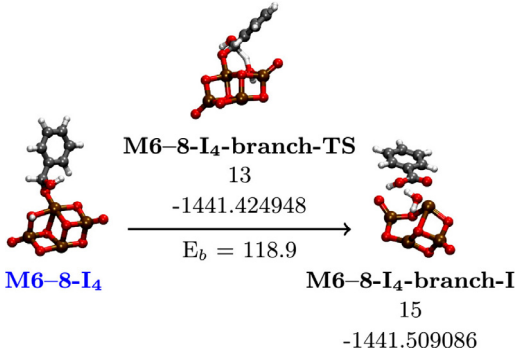

Fig. 7. Energetic profile graph with the optimized fragments of the intermediate surface species I_m and transition state TS involved in parasitic mechanisms: spin multiplicity $(2S+1)$ characterizing the fragments and the ZPVE/hartree values are given in the order under any structure. E_b is the energy barrier, i.e. the energy gap to get TS, see Eq. (1). Pathway mechanism and intermediate from which starts the parasitic route are highlighted in blue. **M6**–**M8** labels indicate surface species and transition state common to the three mechanisms. (For interpretation of the references to color in this figure legend, the reader is referred to the web version of this article.)

The starting not activated adsorption energy value of the mechanisms **M6**–**M8** was put as the inverse of the desorption energy value of the **M3** one.

The discussion on the application of *SCM* reported in the connected article [1] refers to processes occurring at 343 K. Turn-over frequency (*TOF*) was calculated at the same temperature [1] by using Eq. (16) (see Section 2.2).

Table 2
Surface molar ratios (θ_i) of intermediates and free active sites and probabilities per unit of time ($w_{\pm i}$) of the elementary events involved in the $\Phi CH_2OH \rightarrow [Mn_4O_8]\Phi CHO$ **M1** pathway, at different temperatures (T).

T/K	θ_1[a]	$\mathbf{w_{+1}}\|\mathbf{w_{-1}}$[b]/s^{-1}	θ_2	$\mathbf{w_{+2}}\|\mathbf{w_{-2}}$/s^{-1}	θ_3	$\mathbf{w_{+3}}\|\mathbf{w_{-3}}$/s^{-1}	θ_4	$\mathbf{w_{+4}}\|\mathbf{w_{-4}}$/s^{-1}	$\mathbf{s}$[c]/s^{-1}
321	$9.\times10^{-19}$	$7.\times10^{12}\|8.\times10^{-13}$	$9.\times10^{-6}$	$4.\times10^{6}\|4.\times10^{7}$	$9.\times10^{-7}$	$7.\times10^{0}\|1.\times10^{-14}$	$1.\times10^{0}$	$6.\times10^{-6}\|0.\times10^{0}$	6.1×10^{-6}
343	$1.\times10^{-17}$	$7.\times10^{12}\|4.\times10^{-11}$	$2.\times10^{-5}$	$1.\times10^{7}\|1.\times10^{8}$	$2.\times10^{-6}$	$5.\times10^{1}\|7.\times10^{-13}$	$1.\times10^{0}$	$9.\times10^{-5}\|0.\times10^{0}$	9.4×10^{-5}
398	$3.\times10^{-15}$	$8.\times10^{12}\|7.\times10^{-8}$	$8.\times10^{-5}$	$8.\times10^{7}\|5.\times10^{8}$	$1.\times10^{-5}$	$2.\times10^{3}\|2.\times10^{-9}$	$1.\times10^{0}$	$2.\times10^{-2}\|0.\times10^{0}$	2.3×10^{-2}
420	$2.\times10^{-14}$	$9.\times10^{12}\|8.\times10^{-7}$	$1.\times10^{-4}$	$2.\times10^{8}\|9.\times10^{8}$	$2.\times10^{-5}$	$6.\times10^{3}\|3.\times10^{-8}$	$1.\times10^{0}$	$1.\times10^{-1}\|0.\times10^{0}$	1.4×10^{-1}

[a] θ_1 represents the surface molar ratio of the free active surface site. A given θ_i that of the surface intermediate I_{i-1}.
[b] For a given process $X_i \Leftrightarrow X_j$, w_{+i} and w_{-i} correspond (see note in Section 2.2) to w_{ij} and w_{ji}, respectively.
[c] Reaction rate is expressed in molecule converted per unit of time per catalytic Mn_4O_8 fragment.

Table 2 reports the surface molar ratios of the free active sites and of the intermediates involved, at given temperatures, in an example pathway, summing up the *SCM* approach. The table, with the whole pathway reaction rate, also shows the probabilities of occurrence per unit of time of the simple events that characterize the pathway itself. In passing, it is observed that the Arrhenius plot of the pathway can be obtained [1], using data of the first and last column.

1.3. Supplementary material

Optimized cartesian coordinates for all the species considered in Figs. 1–7, reported in Section 1.1, are included as electronic supplementary material. Before each structure coordinates, the names, the same ones employed in the figures, and the corresponding zero-point corrected absolute energies (in hartree) are shown. All the minima and transition states were optimized using the Berny geometry optimization algorithm [3].

2. Experimental Design, Materials and Methods

2.1. Structure and energetic data: models and methods

Geometry optimization and harmonic frequency calculation of all the compounds reported in this article were performed within the Density Functional Theory framework by using the M06L exchange-correlation functional, joined with the Stuttgart '97 Relativistic Small Core effective potential and the corresponding valence double zeta basis set for Mn atoms, and the correlation-consistent polarized double zeta basis set (cc-pVDZ) for H, C and O atoms. M06L [4] is a standalone meta generalized gradient approximation exchange-correlation functional belonging to the M06 family developed by Zao and Truhlar. The Stuttgart '97 Relativistic Small Core effective potential is a pseudopotential which describes the 10 innermost electrons of manganese atom with gaussian-like functions up to f angular momentum, coupled with a (8s7p6d1f)/[6s5p3d1f] contraction scheme valence basis set [5,6]. Developed by Dunning, the cc-pVDZ [7] is an all-electron double zeta valence basis set, which belongs to the cc-pVNZ series (N = D, T, Q, 5, 6, 7); it has (5s2p)/[2s1p] contraction scheme for hydrogen and (19s5p1d)/[3s2p1d] for carbon and oxygen. For DFT calculations, performed with the D.01 version of the Gaussian 09 suite of program [8], an integration grid formed by 99 radial points and 590 angular points was used. The nature of transition states was checked by inspection of the normal mode corresponding to the unique imaginary frequency. Inputs structures for electronic structure calculations and outputs of the final geometries were managed by the Molden code [9]. All molecular graphical representations reported throughout were realized by using VMD [10] and composed by means of the TikZ package in Latex.

2.2. Modeling experimental design to get kinetic data

Kinetic data have been obtained employing an original simplified approach derived by the classical method introduced in 1953 by Christiansen [11]. In this, the problem of reconstructing the mechanism of a given reaction by determining its elementary steps is deepened.

The elementary steps, in fact, can be combined to determine different reaction pathways which in turn can play a more or less important (or even null) role in the reaction stoichiometry occurrence. The article was mainly aimed at experimentalists involved in catalysis who, through kinetic approaches, could obtain the descriptors, mostly kinetic constants and species concentrations, useful for arriving at the mechanistic solution of the system under examination. Kinetic constants were presented as the probability of occurrence of the corresponding events per unit of time.

More recently it has been observed by Kozuch and Shaik [12] that if free energies (or other computable related parameters, such as the vibrational zero-point corrected energy barrier) of all the species involved in a catalytic process were affordable through computation, Christiansen's approach could be employed also for the theoretical determination of experimental quantities such as the TOF values of the reaction.

In the present work, the Christiansen's method, simplified to a certain extent and therefore here defined *reduced*, was used to compare the occurrence probabilities either of different surface reaction paths, contributing to a given process stoichiometry, or of different surface processes, when potentially occurring in parallel on the same active sites.

The approach used is shortly summarized below, recalling that the dimensions of the physical quantities involved will not generally be represented, as they are easy to understand. As a further premise, it is stated that the occurrence probability per unit of time, w/s^{-1}, of a given elementary step, involving any surface reaction species, was calculated by the Eyring's equation:

$$w = \kappa \frac{K_B T}{h} exp\left(-\frac{E_b}{RT}\right)$$

where besides R, K_B, h and T that have the usual meaning, κ, always considered very close (and practically equal) to 1, is the transmission coefficient and E_b, which replaces the free energy term $\Delta G^{\ddagger}$ present in the original version of the Eyring's equation, the vibrational zero-point corrected energy barrier [12], individuating the energy of the transition state of a given elementary step. Incidentally, it is finally recalled that the unit of time, τ, not explicitly used in the following, could be expressed as the inverse of the pre-exponential term of the equation above: $\tau = \frac{h}{K_B T}$. Thus, the pre-exponential term clearly gives the dimension to w.

The E_b descriptors for the title catalytic systems are reported in Table 1 in the **TS** columns and in Figs. 4–7 for some parasitic pathway. While w data, at different temperatures, for the elementary steps involved in the pathway **M1** of Table 1: $\Phi CH_2OH \rightarrow [Mn_4O_8]\Phi CHO$, are shown, as an example, in Table 2.

Then, referring to the catalytic systems treated in the present work, suppose having a set of n elementary steps, involving given species, which define a given reaction path that shapes the stoichiometric surface reaction R $\Leftrightarrow$ P, characterized by $n-1$ $\mathbf{I}_i$ surface intermediates:

$$\mathrm{R} + \Omega \underset{[w_{-1}]}{\overset{[w_1]}{\Longleftrightarrow}} \mathbf{I}_2 \quad \mathbf{I}_2 \underset{[w_{-2}]}{\overset{[w_2]}{\Longleftrightarrow}} \mathbf{I}_3 \quad \mathbf{I}_3 \underset{[w_{-3}]}{\overset{[w_3]}{\Longleftrightarrow}} \mathbf{I}_4 \ldots\ldots \mathbf{I}_n \underset{[w_{-n}]}{\overset{[w_n]}{\Longleftrightarrow}} P + \Omega \tag{3}$$

being Ω the not occupied active surface site, the corresponding set of kinetic equation is:

$$\begin{aligned} &\theta_1 w_1 \rho - \theta_2 w_{-1} = s_1 \\ &\theta_2 w_2 - \theta_3 w_{-2} = s_2 \\ &\theta_3 w_3 - \theta_4 w_{-3} = s_3 \\ &\ldots\ldots\ldots\ldots\ldots\ldots \\ &\theta_n w_n - \theta_1 w_{-n} \pi = s_n \end{aligned} \tag{4}$$

where ρ and π are generic concentrations of the starting reactant R and the final product P, respectively, and s_i the rates characterizing the single elementary steps. While, θ_i is the fraction either of the not occupied active sites ($i = 1$) or of the remaining surface sites, occupied by given ith ($i \neq 1$) species $\mathrm{I_i}$, hence:

$$\Theta = \sum_{i=1}^{n} \theta_i = 1$$

In passing, it is said here that the notation θ_1, for the not occupied surface site fraction, instead of the more usual θ_0 is used for convenience since in this way the following matrix notations look particularly simple. Other than the notational convenience, it is still possible to write $\theta_1 = \theta_0$.

In presence of quasi-stationary conditions [11] it can be written $s_1 = s_2 = \ldots = s_n = s$, being s the whole reaction rate. Setting $\rho w_1 = \bar{w}_1$ and $\pi w_{-n} = \bar{w}_{-n}$, the equation system (4) can be

written as:

$$\begin{aligned}
&\frac{\theta_1}{s}\bar{w}_1 - \frac{\theta_2}{s}w_{-1} = 1\\
&\frac{\theta_2}{s}w_2 - \frac{\theta_3}{s}w_{-2} = 1\\
&\frac{\theta_3}{s}w_3 - \frac{\theta_4}{s}w_{-3} = 1\\
&\cdots\cdots\cdots\cdots\cdots\\
&\frac{\theta_n}{s}w_n - \frac{\theta_1}{s}\bar{w}_{-n} = 1
\end{aligned} \tag{5}$$

and in matrix notation (5) becomes:

$$\frac{1}{s}\begin{bmatrix} \bar{w}_1 & -w_{-1} & 0 & \dots & 0\\ 0 & w_2 & -w_{-2} & \dots & 0\\ 0 & 0 & w_3 & \dots & 0\\ \dots & \dots & \dots & \dots & \dots\\ \bar{w}_{-n} & 0 & 0 & \dots & w_n \end{bmatrix}\begin{bmatrix} \theta_1\\ \theta_2\\ \theta_3\\ \dots\\ \theta_n \end{bmatrix} = \begin{bmatrix} 1\\ 1\\ 1\\ \dots\\ 1 \end{bmatrix} \tag{6}$$

The determinant $det(L)$ from the $n \times n$ matrix L present in (6) can be trivially obtained:

$$det(L) = \bar{w}_1 w_2 w_3 \dots w_n - \bar{w}_{-n} \dots w_{-3} w_{-2} w_{-1} = \rho w_1 w_2 w_3 \dots w_n - \pi w_{-n} \dots w_{-3} w_{-2} w_{-1} \tag{7}$$

Instead of solving the system that characterizes a given pathway from time to time, Christiansen identifies (and suggests to use) a matrix with a peculiar notation, having mnemonic purposes, indicated as M and called, due to its properties, partition matrix.

M is aimed at identifying the solution of a generic system of kinetic equations in a simple and systematic way. It has dimensions $n \times n$ and each of its term is made by the product of $n-1$ probabilities per unit of time (which will be referred, in order to simply, as probabilities, in the following). The first term in the first column is $w_2 w_3 \dots w_n$, the subsequent terms in the same column are obtained by increasing both positive and negative (if present) indices of the single probabilities that ideally precede them (in the term above) by one unit and restarting from 1 or -1 if the above probability reached the index n or $-n$, respectively. The second and the last (nth) term of the first column, as an example, will be, $w_3 w_4 \dots \bar{w}_1$ and $\bar{w}_1 w_2 \dots w_{n-1}$, in the order.

The first term of the second column is obtained by substituting just the first probability of the first term of the first column, w_2, with w_{-1}, thus obtaining $w_{-1} w_3 \dots w_n$. The first term of the third column is obtained, instead, by exchanging only the second probability of the first term of the second column, w_3, with w_{-2}, thus obtaining $w_{-1} w_{-2} \dots w_n$. It is possible to proceed further with the first terms of the following $(i+1)$th column, substituting only the ith probability in the first term of the preceding ith column with the probability w_{-i}, thus obtaining $w_{-1} w_{-2} \dots w_{-i} \dots w_n$. This is done up to the last column, whose first term therefore is $w_{-1} w_{-2} \dots w_{-i} \dots w_{-(n-1)}$. The rules already given for the completion of the first column are conversely used to introduce the remaining $n-1$ terms of the remaining columns. The M matrix relating to a pathway of 3 elementary steps is shown below:

$$M = \begin{Vmatrix} w_2 w_3 & w_{-1} w_3 & w_{-1} w_{-2}\\ w_3 \bar{w}_1 & w_{-2} \bar{w}_1 & w_{-2} \bar{w}_{-3}\\ \bar{w}_1 w_2 & \bar{w}_{-3} w_2 & \bar{w}_{-3} w_{-1} \end{Vmatrix}$$

Apart from the construction method, the mnemonic characteristics of the M matrix are evident considering the sum of all the terms in the different rows i, $|M_i|$, and observing that the solution of the system (5) can be summarized as:

$$\frac{|M_i|}{det(L)} = \frac{\theta_i}{s} \tag{8}$$

It should be, at this point, noted that M simplifies when one or more probabilities are equal or close to zero and in particular when $\bar{w}_{-n} \cong 0$, condition which corresponds to the occurrence of an irreversible R → P process. In this case, all the terms containing $\bar{w}_{-n}$ are, indeed, zeroed and L hence $det(L)$ simplify. This in its *reduced* form, in particular, becomes:

$$det_R(L) = \bar{w}_1 w_2 \dots w_n = \prod_{i=1}^{n} w_i = \Lambda \tag{9}$$

In passing, two items may be pointed out:

i) a variant of (9), which will not be used here anyway, could be obtained by setting $\theta_1 = \rho \cdot \theta_0$ in (6). This position provides a further simplified equation, characterized by the substitution of $\bar{w}_1$ with w_1 in (9);
ii) even if the starting catalytic fragment is modified by the surface processes ($\Omega \rightarrow \Omega^*$), the here matrix approach can be still used. In fact, the corresponding initial and final surface molar ratio, for Ω and Ω^*, can be written as $(1-\zeta)\cdot\theta_1$ and $\zeta \cdot \theta_1$, being $\zeta \leq 1$. Of course, coefficients $(1-\zeta)$ and ζ can be included, separately and in the order, in the $\bar{w}_1$ and $\bar{w}_{-n}$ terms present in the set (5). As a consequence, $\bar{w}_1$ and $\bar{w}_{-n}$ will strictly depend (see below) on the properties of the catalytic system and conditions of use of the catalyst.

In any case, the system (8) can be solved by a new set of equations:

$$\frac{|M_i|}{\Lambda} = \frac{\theta_i}{s} \tag{10}$$

where θ_1 is equal either to θ_0 or to $\rho \cdot \theta_0$ and as a consequence in $|M_i|$ and Λ is used $\bar{w}_1$ or w_1, depending on the simplification level introduced.

The occurrence of irreversible reactions is quite common in heterogeneous catalysis and not only, as already underlined by Christiansen [11].

Assuming, as an example, to model a continuous flow process with a rich reactant feedstock that makes the concentration of the product and therefore its adsorption negligible, the reaction itself can be considered as irreversible. These conditions in addition guarantees that the non-activated adsorption (typical of the species considered in the title reaction) of the largely present starting reactants is just determined by the presence of free active sites, therefore by the extent of their $(\theta_1 = \theta_0)$ fraction. Due to both the observations above, only the case in which for any single pathway the restricting conditions $\theta_1 = \theta_0$, $\bar{w}_{-n} \cong 0$ and $\bar{w}_1 = \frac{k_B T}{h}$ will be further examined, being $\frac{k_B T}{h}$ the probability of not dissociative (hence not activated) adsorption step per unit of time at a given temperature T.

Then, being $\Xi = s/\Lambda$, with Ξ constant in the different equations of the system (10), setting $|M| = \sum_{i=1}^{n} |M_i|$, it will be:

$$\sum_{i=1}^{n} \theta_i = \Xi \sum_{i=1}^{n} |M_i| = 1 \tag{11}$$

that is:

$$\Xi = \frac{1}{|M|} \tag{12}$$

and:

$$s = \frac{\Lambda}{|M|} \tag{13}$$

while, employing any equation of the system (10), from (12):

$$\theta_i = \frac{|M_i|}{|M|} \tag{14}$$

In case there are surface processes that modify either structural or compositional and/or topological properties of the catalyst ($\Omega \rightarrow \Omega^*$), $\bar{w}_1$ will include the parameter ζ, see item *ii*) above. This is, in most cases, not a problem in the kinetic system analysis since ζ is typically negligible with respect to 1; as an example, in the case characterizing the initial phases of a reaction involving surface processes, already at kinetic regime, in which the reagent desorption is strongly endergonic. Due to the properties of the pathways involved in the title reaction (see Table 1), only these conditions were considered in the connected article [1].

In Table 1, along with the relative energetics of the surface species and transition states involved in significant pathways composing the final mechanisms of the title reaction, are outlined the most abundant surface species, Θ, and the whole reaction rate (see below) of the different

pathways, at 398 K whereas the θ values of the different species involved in the benzyl alcohol oxidation to benzaldeide: $\Phi CH_2OH \rightarrow [Mn_4O_8]\Phi CHO$, at different temperatures, as already stated, are reported in Table 2 with the corresponding whole reaction rate, s and with the probabilities of occurrence per unit of time, $w_{\pm i}$, of any single step.

It has to be stressed that Eqs. (13) and (14) allow one to obtain from computed energy barriers, thus from the probabilities correlated to them, either the reaction rates or the corresponding different fractions of active sites occupied or not and with this to have a panorama in the trend of the surface population during the reaction, which could potentially give an address on possible changes, in order to modify the process and namely its activity and selectivity.

Furthermore, from the comparison of the rates, s, characterizing different paths that concur to determine the same stoichiometric process $R \Leftrightarrow P$ the most probable of these can be determined (the one with the highest reaction rate). Whereas, having different reactions $R_i \Leftrightarrow P_i$ occurring on the same catalytic sites, employing the same criteria, it is possible to have an idea of their relative rates and therefore of the selectivity towards the single processes.

A system that evolves through non-activated steps deserves further consideration. One case is for example represented by non-dissociative (hence not activated) adsorption. Using the notation introduced in (5), it can be written:

$$s_1 = \theta_1 \bar{w}_1 - \theta_2 w_{-1} \tag{15}$$

Recalling that not activated processes are characterized by exponential terms equal to 1 in the Eyring's equation and since at time $t = 0$ $\theta_1 = 1$ and $\theta_2 = 0$, it is clear that the adsorption rate, as already mentioned, depends only on $\bar{w}_1 = \frac{k_B T}{h}$, which is constant, at a given temperature, irrespective of the process energetics when the same starting reagent concentration is considered. At times $t \neq 0$, s_1 is conversely determined by w_{-1}, therefore by the desorption energetics, which can also have a role at the equilibrium, i.e. when $s = s_1$, in determining the reaction rate of the whole process.

Fig. 8a illustrates another case.[1] which could actually arise when, as an example, free rotation occurs to interconvert given intermediates X_1 and X_2, before the latter transforms into X_3. In this case, the probabilities referable to X_1 and X_3 can be calculated as usual through the Eyring's equation. Also the probability w_{23} referable to the X_2 conversion into X_3 can be evaluated in the same way. The probability of going back to X_1 from X_2, w_{21}, is instead calculated as $w_{21} = \frac{k_B T}{h} - w_{23}$. It has to be noticed that in this case the *null event* probability w_{22} (see footnote) is equal to 0.

That probability is, conversely, involved in the most common cases shown in Fig. 8b. In fact, recalling that the probabilities of X_2 evolving into X_1 or X_3 are w_{21} and w_{23}, respectively, there is a probability that nothing happen, $w_{22} = \frac{k_B T}{h} - [w_{21} + w_{23}] \neq 0$, which characterizes X_2 and more generally $w_{ii} = \frac{k_B T}{h} - [w_{i(i-1)} + w_{i(i+1)}] \neq 0$, for a given X_i species.

A final case, although not explicitly involved in the title reaction system, needs to be considered. Fig. 8c shows the notable case of a *labile* intermediate X_2 that is characterized by a maximum in the reaction profile of a given surface process (e.g. desorption of one species followed by non-dissociative adsorption of another species on the same site or of the same species on another site). In this case, the probabilities of the processes $X_1 \rightarrow X_2$ and $X_3 \rightarrow X_2$ will follow what has already been outlined above, on the contrary the processes $X_2 \rightarrow X_1$ and $X_2 \rightarrow X_3$ will be characterized, employing the usual notation already introduced, by the probabilities $w_{21} = w_{23} = \frac{1}{2}\frac{k_B T}{h}$, being the null probability $w_{22} = 0$, once more.

It is yet interesting to point out that knowing the dispersion D_χ of a given heterogeneous catalyst, defined as the ratio between effectively and potentially active catalytic sites, a given

[1] To discuss the cases in Fig. 8, it is more convenient to change notations for the probabilities per unit of time. As an example, for the forward and backward transformations $X_i \Leftrightarrow X_j$ instead of w_{+i} and w_{-i} we will use w_{ij} and w_{ji}. A particular case, usually not taken into consideration, is represented by the probability that nothing will happen (null event probability). This will be represented as w_{ii} and w_{jj} for the two events above.

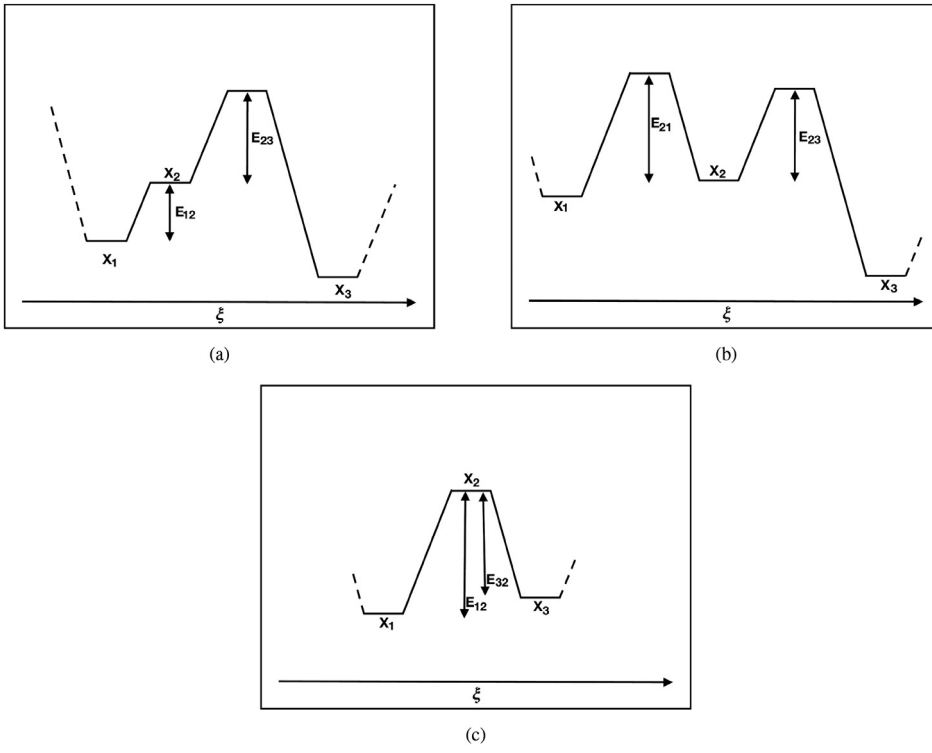

Fig. 8. Energy scheme representation of different reaction spots. (a) X_1 undergoes to a structural rearrangement, like a free rotation, before converting to X_3; (b) the conversion from X_1 to X_3 occurs through the formation of the X_2 intermediate; (c) a labile intermediate, X_2, is a maximum along the reaction profile. X_i represents a given surface species, ξ is the reaction coordinate while E_{ij} is the energy barrier needing in the $X_i \rightarrow X_j$ process.

calculated reaction rate, s, could be related to an estimate of the corresponding TOF/s^{-1} by:

$$TOF = \frac{s}{D_\chi} \tag{16}$$

The modeling experimental design developed so far, surely simplified by the approximations introduced, is rather easy to be followed. Its generalization, always referred to the identification of the quantities referred to in Eqs. (13) and (14), is however quite simple and easily implemented in a calculation code or, as in the present case, in a computer algebra system (CAS) like Maxima [13]. The reduced form of the Christiansen's method already indicated as *SCM* [1], acronym for Simplified Christiansen Method, has been here used to obtain data reported in Tables 1 and 2.

Declaration of Competing Interest

The authors declare that they have no known competing financial interests or personal relationships which have, or could be perceived to have, influenced the work reported in this article.

CRediT Author Statement

Laura Gueci: Conceptualization, Formal analysis, Investigation, Data curation, Writing – original draft; **Francesco Ferrante:** Conceptualization, Methodology, Software, Validation, Data cura-

tion, Writing – review & editing, Visualization; **Antonio Prestianni:** Conceptualization, Visualization; **Francesco Arena:** Conceptualization, Validation; **Dario Duca:** Conceptualization, Methodology, Software, Validation, Formal analysis, Resources, Writing – review & editing, Supervision, Project administration, Funding acquisition.

Acknowledgments

University of Palermo is thanked for the policy of supporting Open Access publications.

Supplementary Material

Supplementary material associated with this article can be found in the online version at doi:10.1016/j.dib.2021.107369

References

[1] L. Gueci, F. Ferrante, A. Prestianni, F. Arena, D. Duca, Benzyl alcohol to benzaldehyde oxidation on MnO_x clusters: unraveling atomistic features, Mol. Catal. 513 (2021) 111735.
[2] L. Gueci, F. Ferrante, A. Prestianni, R. Di Chio, A.F. Patti, D. Duca, F. Arena, DFT insights into the oxygen-assisted selective oxidation of benzyl alcohol on manganese dioxide catalysts, Inorg. Chim. Acta 511 (2020) 119812.
[3] H.G. Schlegel, Optimization of equilibrium geometries and transition structures, J. Comput. Chem. 3 (1987) 214–218.
[4] Y. Zhao, D.G. Truhlar, A new local density functional for main-group thermochemistry, transition metal bonding, thermochemical kinetics, and noncovalent interactions, J. Chem. Phys. 125 (2006) 194101.
[5] M. Dolg, U. Wedig, H. Stoll, H. Preuss, Energy-adjusted ab initio pseudopotentials for the first row transition elements, J. Chem. Phys. 86 (1987) 866–872.
[6] J.M.L. Martin, A. Sundermann, Correlation consistent valence basis sets for use with the Stuttgart–Dresden–Bonn relativistic effective core potentials: the atoms Ga–Kr and In–Xe, J. Chem. Phys. 114 (2001) 3408–3420.
[7] T.H. Dunning, Gaussian basis sets for use in correlated molecular calculations. I. The atoms boron through neon and hydrogen, J. Chem. Phys. 90 (1989) 1007–1023.
[8] M.J. Frisch, G.W. Trucks, H.B. Schlegel, G.E. Scuseria, M.A. Robb, J.R. Cheeseman, G. Scalmani, V. Barone, B. Mennucci, G.A. Petersson, H. Nakatsuji, M. Caricato, X. Li, H. P. Hratchian, A. F. Izmaylov, J. Bloino, G. Zheng, J.L. Sonnenberg, M. Hada, M. Ehara, K. Toyota, R. Fukuda, J. Hasegawa, M. Ishida, T. Nakajima, Y. Honda, O. Kitao, H. Nakai, T. Vreven, J. J. A. Montgomery, J.E. Peralta, F. Ogliaro, M. Bearpark, J.J. Heyd, E. Brothers, K.N. Kudin, V.N. Staroverov, R. Kobayashi, J. Normand, K. Raghavachari, A. Rendell, J.C. Burant, S.S. Iyengar, J. Tomasi, M. Cossi, N. Rega, J.M. Millam, M. Klene, J.E. Knox, J.B. Cross, V. Bakken, C. Adamo, J. Jaramillo, R. Gomperts, R.E. Stratmann, O. Yazyev, A.J. Austin, R. Cammi, C. Pomelli, J.W. Ochterski, R.L. Martin, K. Morokuma, V.G. Zakrzewski, G.A. Voth, P. Salvador, J.J. Dannenberg, S. Dapprich, A.D. Daniels, O. Farkas, J.B. Foresman, J.V. Ortiz, J. Cioslowski, D.J. Fox, (2013). Gaussian 09 Revision D.01. Gaussian Inc. Wallingford CT 2009.
[9] G. Schaftenaar, J.H. Noordik, Molden: a pre- and post-processing program for molecular and electronic structures, J. Computer-Aided Mol. Des. 14 (2000) 123–134.
[10] W. Humphrey, A. Dalke, K. Schulten, VMD - visual molecular dynamics, J. Mol. Graph. 14 (1996) 33–38.
[11] J.A. Christiansen, The elucidation of reaction mechanisms by the method of intermediates in quasi-stationary concentrations, Adv. Catal. 5 (1953) 311–353.
[12] S. Kozuch, S. Shaik, A combined kinetic-quantum mechanical model for assessment of catalytic cycles: application to cross-coupling and heck reactions, J. Am. Chem. Soc. 128 (2005) 3355–3365.
[13] W. Schelter, (2021). Maxima, a Computer Algebra System. Version 5.45.0. http://maxima.sourceforge.net/.